

Diagnostic Ultrasound Image Enhancement: A Multiscale Permutation Approach

S. Kalaivani

Department of Electronics and Communication Engineering, T.R.P. Engineering College (SRM Group), Irungalore,
Trichirappalli, Tamilnadu, India
E-mail: s_kalai@rediffmail.com

R. S. D. Wahidabanu

Department of Electronics and Communication Engineering, Government College of Engineering,
Salem, Tamil Nadu, India

Abstract. It has been estimated that one out of every four medical diagnosis in the world involves ultrasound imaging modality because of its noninvasive nature, low cost and capability of forming real time imaging. Ultrasonic imaging extends its application to many fields of medical diagnosis, but the utilization is being unfortunately affected by speckle noise. In this article, an efficient multiscale approach is proposed to reduce speckle, to enhance the edge information and to preserve point and linear features, rather than just inhibiting smoothing. With this approach, the image enhancement is made in three steps: First the image is transformed into Laplacian pyramid domain representation. Second, the pyramid coefficients are manipulated by permuted diffusion, and finally the image is reconstructed from the diffused Laplacian pyramid. New permuted diffusion is proposed for coefficient manipulation for effective speckle reduction and enhancement. The proposed permuted diffusion avoids the blocky effects caused by second-order partial differential equation (PDE) and requires only little iteration compared to fourth-order PDE to converge. In each pyramid layer, a gradient threshold is estimated automatically using robust median estimator. The mean absolute error between two adjacent diffusion steps is used as a stopping criterion. Performance of the proposed approach is compared with the state of the art pyramid based methods. Experiments on synthetic data, simulated phantom and real ultrasound data set indicate effective suppression of speckle, preservation of edge information and their structural details. © 2012 Society for Imaging Science and Technology.

[DOI: 10.2352/J.ImagingSci.Technol.2012.56.1.010501]

INTRODUCTION

Ultrasound Medical imaging is very popular due to its low cost, least harmful to human body, real time view, and small size. It is estimated that one out of every four medical diagnostic image studies in the world involves ultrasonic techniques. Ultra sound (US) waves are characterized by frequency above 20 kHz, which is the upper limit of human hearing. In medical US applications, frequencies are used between 500 kHz and 30 MHz. B-mode imaging is the most preferred modality in medical US. When an US transducer placed

onto the patient's skin over the imaged region, it sends a US pulse that travels along a beam into the tissue. Due to interfaces some of the US energy is reflected back to the transducer and converted into echo signals. These signals are then sent into the amplifiers and signal processing circuits in the imaging machine's hardware to form a 2D image. The process of launching pulses in different directions is repeated in order to examine the whole region in the body. Thus, US imaging involves signals which are obtained by coherent summation of echo signals from scatterers in the tissue.

ULTRASOUND IMAGING SYSTEM

The functional block diagram of an ultrasound imaging system is depicted in Figure 1. The construction of ultrasound B-mode image involves capturing of echo signal returned from the tissue at the surface of piezoelectric crystal transducers. These transducers convert the ultrasonic RF mechanical wave into electrical signal. Convex ultrasound probes collect the echo from the tissue in a radial form. Each group of transducers is simultaneously activated to look at a certain spatial direction from which they generate a raw line signal called A-line, which is later used for raster image construction. These A-lines are then demodulated and logarithmically compressed to reduce their dynamic range to suit the commercial display devices. The final Cartesian image is constructed from the sampled A-lines in a process called scan conversion.

Speckle reduction techniques can be applied on envelope detected data, log compressed data, or on scan converted data. However, slightly different results will be produced for each data. In the compression stage, some useful information about the imaged object may be deteriorated or even lost. For optimum result envelope detected data processing is preferred because some information that lost after the compression stage cannot be recovered by working with log compressed data or the scan converted image. However, the real time speckle reduction methods

Received May 25, 2011; accepted for publication Nov. 1, 2011; published online Mar. 15, 2012.

1062-3701/2012/56(1)/010501/12/\$20.00.

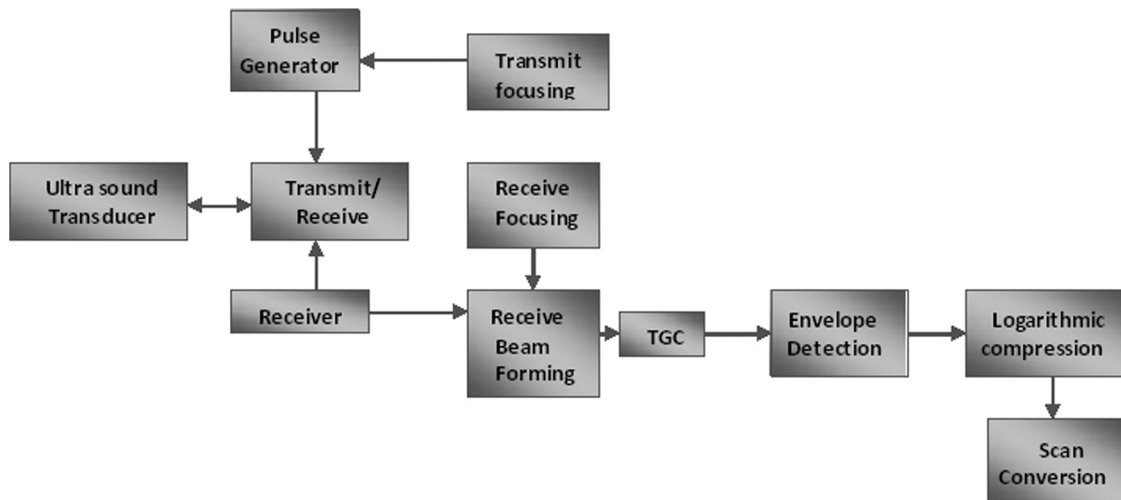


Figure 1. Block diagram of ultrasound imaging system.

are applied on the scan converted image, since the scan converted image is always accessible and most of the commercial ultrasound systems do not output the envelope detected or log compressed data.

SPECKLE IN ULTRASOUND IMAGING

Speckle in US B-scan is seen as a granular structure, which is caused by the constructive and destructive coherent interferences of back scattered echoes from the scatterers that are typically much smaller than the spatial resolution of medical ultrasound system.^{1,2} This phenomenon is common to laser, sonar, and synthetic aperture radar imagery.³ Speckle pattern is a form of multiplicative noise, and it depends on the structure of imaged tissue and various imaging parameters. Speckle degrades the target detection ability in B-scan images and reduces the contrast, resolutions. This affects the human ability to identify normal and pathological tissues. It also degrades the speed and accuracy of ultrasound image processing tasks such as segmentation and registration.

The nature of the speckle pattern can be categorized into one of three classes according to the number of scatterers per resolution cell or the so called scatterer number density, spatial distribution and the characteristics of the imaging system itself. These classes are described as follows:

- (1) Fully formed speckle pattern: It occurs when many fine randomly distributed scattering sites exist within the resolution cell of the pulse-echo system. In this case, the amplitude of the backscattered signal can be modeled as a Rayleigh distributed random variable⁴ with a constant SNR of 1.92. Blood cells are typical examples of this type of scatterers.
- (2) Nonrandomly distributed with long-range order: Examples of this type are the lobules in liver parenchyma. It contributes a coherent or specular backscattered intensity that is in itself spatially varying. Due to the correlation between scatterers, the effective number of scatterers is finite. This situa-

tion can be modeled by the K-distribution. This type is associated with SNR below 1.92. It can also be modeled by the Nakagami distribution.^{5,6}

- (3) Nonrandomly distributed with short-range order: Examples of this type include organ surfaces and blood vessels. When a spatially invariant coherent structure is present within the random scatterer region, the probability density function of the backscattered signals becomes close to the Rician distribution.⁷ This class is associated with SNR above 1.92.

Thus, speckle is considered as the dominant source of noise in ultrasound imaging and should be processed without affecting important image features. The main purposes for speckle reduction in medical ultrasound imaging are (1) To improve the human interpretation of ultrasound images—speckle reduction makes an ultrasound image cleaner with clearer boundaries and (2) Despeckling is a preprocessing step for many ultrasound image processing tasks such as segmentation and registration—speckle reduction improves the speed and accuracy of automatic and semiautomatic segmentation and registration. The following factors have to be taken into account in developing an efficient and robust denoising method for ultrasound images.

Adaptation to Features of Interest

For an experienced radiologist speckle noise (also referred as “texture” in medical literature) may present diagnostic information. The degree of speckle smoothing depends on the expert’s knowledge and the application at hand, like enhancement for visual inspection or preprocessing for automatic segmentation. For automatic segmentation, it is usually preferred to keep the sharpness of the boundaries between different image regions and to smooth out the speckle texture. For visual interpretation, the texture smoothing may be less preferable.

Adaptive to Spatial Content

The medical ultrasound images have significant spatial correlation. A spatially adaptive denoising can be based on statistical content models or on adapting certain filter parameters based on measurements from a local window around each pixel.

Proposal of Noise Models

The basic assumption in majority of speckle filters is that the speckle is fully developed and is modeled as multiplicative noise. Logarithmic operation transforms speckle into additive white Gaussian noise. But for different reasons such a speckle model seems to be too simplistic in the case of medical ultrasound images. Speckle is not necessarily being fully developed and there exists a pronounced spatial correlation. Moreover, the ultrasound devices themselves usually perform a preprocessing of the raw data including even logarithmic compression. Thus, in the displayed medical ultrasound images, the noise differs significantly from often assumed multiplicative method.

Most speckle filters are developed for enhancing visualization of speckle images.^{8–10} In compounding method, a series of ultrasound images of the same target are acquired from different scan directions and with different transducer frequencies or under different strains. Then, the images are averaged to form a composite image. The compounding method can improve the target detection ability but they suffer from degraded spatial resolution and an increased system complexity. Whereas the postacquisition method do not require many hardware modification. The postacquisition image processing technique falls under two categories (1) single scale spatial filtering and (2) multiscale methods. A speckle reduction filter that changes the amount of smoothing according to the ratio of local variance to local mean is developed by Bamber and Daft.¹¹ In which, smoothing is increased in homogeneous region where speckle is fully developed and reduced or even avoided in other regions to preserve details. Unsharp masking filter is suggested in Ref. 12, in which the smoothing level is adjusted depending on the statistics of log compressed images but the filters proposed in Refs. 11 and 12 have difficulty in removing speckle near or on image edges. In region growing based spatial filtering methods,^{13–15} it is assumed that the pixels have similar gray level and connectivity are related and likely to belong to the same object or region. After all pixels are allocated to different groups, spatial filtering is performed based on the local statistics of adaptive regions, whose sizes and shapes are determined by the information content of the image. The main difficulty in applying region growing based methods is designing the appropriate similarity criteria for region growing.

The numbers of filters have been developed for despeckling based on the multiplicative model¹⁶ of speckle noise.^{17–20} Filtering based on anisotropic diffusion (AD) is introduced by Perona and Malik (PM)²¹ and his work has made a great influence in this field of research. Later, edge enhancement function is incorporated to generalize PM

diffusion by Wei²² and a nonlinear fourth-order diffusive term is added to reduce staircase effects and to preserve edges²³ by Chan. et al. and Yu and Acton²⁴ have proposed a novel filtering scheme based on the combination of the filters first described by Lee and Frost. The AD equation gives rise to a speckle removal filter called speckle reducing anisotropic diffusion (SRAD). This filter has shown a very good performance with different levels of speckle; however, for thin linear features and point features, SRAD tends to broaden and it needs to be corrected. Regularization methods have been used in real-valued image restoration^{25,26} as well as image reconstruction problems such as medical tomography^{27,28} to obtain improved image estimates in the face of data degradation. The simplest and most common approach is to use quadratic functions of the unknown quantities. These methods lead to computationally straightforward optimization problems, but they suppress the useful features in the resulting imagery, such as edges. Recently, considerable effort has been spent in designing alternative nonquadratic constraints which preserve such features. Methods based on these nonquadratic constraints have been successfully used in edge-preserving regularization in image restoration²⁷ and computer-assisted tomography.^{27–29}

Recently, there has been a great deal of interest in representations that retain spatial localization in the spatial frequency domain. This is achieved by decomposing the image into a set of spatial frequency band pass component images.³⁰ Individual samples of a component image represent image pattern information that is appropriately localized, while the band passed image as a whole represents information about a particular fineness of detail or scale. There is evidence that the human visual system uses such representation and multiresolution schemes that are becoming increasingly popular in machine vision and in image processing in general.

Several multiscale methods based on wavelet and pyramids have been proposed for speckle reduction in ultrasound imaging. The wavelet based speckle reduction methods^{31–36} have difficulty in determining an appropriate threshold, reasonable distribution models and the exact prior knowledge of noise distribution.

Pyramid transform is a multiscale approach used for reducing speckle.^{37,38} Unlike sub-band decomposition in wavelet transform, the approximation and the interpolation filters in pyramid transform have low pass properties so that pyramid transform does not require quadrature mirror filters. Considering the multiplicative nature of speckle, Aiazzi et al.³⁷ introduced a ratio Laplacian pyramid. In this method, the conventional Kuan filter is extended to multiscale domain by processing the interscale layers of the ratio Laplacian pyramid, but it suffers from the noise variance estimation in each interscale layer. Diffusion based Laplacian pyramid is proposed in Ref. 38 which utilizes the second-order nonlinear diffusion and median absolute deviation estimator. But the use of second-order partial differential equations (PDE) introduces blocky effects and cause broadening of point and linear features.

In this article, an efficient speckle reduction is proposed for the effectively suppress speckle and at the same time to preserve edges and detailed features in the diagnostic image. The proposed method transforms an image into Laplacian pyramid domain, and the pyramid coefficients are manipulated by permuted diffusion, finally the image is reconstructed from the diffused Laplacian pyramid. The permuted diffusion is the combination of second-order and fourth-order PDE. It avoids the blocky effects caused by second-order PDE and require only little iterations compared to fourth-order PDE.

BACKGROUND

Diffusion in Speckle Reduction

The use of PDE in image processing has grown significantly over the past years. Its basic idea is to deform an image, a curve or a surface in a partial differential equation framework and to approach the expected result as a solution to this equation. Diffusion is generally defined as a physical process that equilibrates concentration differences without creating or destroying mass. This physical observation can be easily cast in a mathematical formulation. The equilibration property is expressed by Flick’s law

$$j = -D.\nabla I. \tag{1}$$

This equation states that a concentration gradient ∇I causes a flux j which aims to compensate for this gradient. The relation between ∇I and j is described by the diffusion tensor D , a positive definite symmetric matrix. The case where j and ∇I are parallel is called isotropic. Then, we may replace the diffusion tensor by a positive scalar-valued diffusivity g . Generally, j and ∇I are not parallel. The diffusion only transport mass without destroying it or creating new mass and is expressed by the continuity equation as

$$\partial_t I = -div j, \tag{2}$$

where t denotes the time. If we plug in Flick’s law into the continuity equation, we end up with the diffusion equation

$$\partial_t I = div (D.\nabla I). \tag{3}$$

This equation appears in many physical transport processes. In the context of heat transfer, it is called heat equation. In image processing we may identify the concentration with the gray value at a certain location. If the diffusion tensor is constant over the whole image domain, it is called homogeneous diffusion, and a space-dependent filtering is called inhomogeneous. Often the diffusion tensor is a function of the differential structure of evolving image itself. Such a feedback leads to nonlinear diffusion filters. Diffusion which does not depend on the evolving image is called linear. In general, the homogeneous filtering is named isotropic and inhomogeneous blurring is named as anisotropic. The anisotropic diffusion uses a scalar-valued diffusivity instead of a diffusion tensor. A general expression of the anisotropic diffusion equation can be written as

$$\begin{cases} I(x, 0) = I_0 \\ \frac{\partial I}{\partial t} = div(F) + \beta(I_0 - I) \end{cases}, \tag{4}$$

where F is diffusion and β is data attachment coefficient. Diffusion algorithms remove noise from an image by modifying the image via solving a PDE. For example, applying the isotropic diffusion equation (the heat equation) given by $\partial I(x,y,t)/\partial t = div(c.\nabla I)$, to a noisy image, using the original (degraded or noisy) image $I(x,y,0)$ as the initial condition [where $I(x,y,0); \mathbb{R}^2 = \mathbb{R}^+$ is an image in the continuous domain, (x, y) specifies spatial position, t is an artificial time parameter, c is the diffusion constant, and ∇I is the image gradient] is equivalent to filtering the image with a Gaussian filter.

Second-Order PDE

Second-order PDE have studied as a useful tool for image enhancement and scale space analysis of image. In 1990, Perona and Malik²¹ proposed a nonlinear anisotropic diffusion equation for better image smoothing and his work made an important influence on this field. The PDE of anisotropic diffusion is given as follows in continuous domain:^{17,18}

$$\begin{cases} \frac{\partial I}{\partial t} = \nabla.[c(|\nabla I|)\nabla I] \\ I(t = 0) = I_0 \end{cases}, \tag{5}$$

where ∇ is the gradient operator, $\nabla.$ is the divergence operator, $|\cdot|$ denotes the magnitude, $c(x)$ is the diffusion coefficient, and I_0 is the initial image. But using P-M equation to smooth the image bring in “blocky effects,” i.e., after image progress the gray level in some region is very close or same. 2D SRAD (Ref. 24) takes the format of the PDE of conventional anisotropic diffusion. Given an intensity image $I_0(x,y)$ having none zero-valued intensities over the image domain Ω , the continuous form of SRAD is expressed as follows:

$$\begin{cases} \frac{\partial I(x, y, t)}{\partial t} = \nabla.[c(x, y, : t)\nabla I(x, y, t)] \\ I(x, y : 0) = I_0(x, y), (\partial I(x, y; t)/\partial \Omega = 0 \end{cases}, \tag{6}$$

where $\partial \Omega$ denotes the border of Ω , $c(x)$ is the diffusion coefficient, and q is the instantaneous coefficient of variation (ICOV). 2D SRAD inherits the partial differential equation format of the conventional anisotropic diffusion and exploits ICOV. 2D SRAD is based on traditional anisotropic diffusion, which is a nonlinear filtering method that encourages diffusion in the homogeneous region, while inhibits diffusion at edges.

Fourth-Order PDE

Second-order PDE based methods tend to cause blocky effects in the image. These effects are visually unpleasant, and there is high possibility of detecting them as false edges by edge detection algorithm. The second-order PDE are usually designed to evolve faster in smooth areas than around the

image edges in order to preserve edges and to remove noise. Therefore, after certain time of evolution, the image will look like one consisting of level areas of various intensities and boundaries and these level areas may coincide with edges.

The fourth-order partial differential equation is proposed in Refs. 39–41. This equation can reduce the noise and at the same time it can keep the image edge better. The fourth-order PDE is

$$\frac{\partial I}{\partial t} = -\nabla^2 [g(|\nabla^2 I|)\nabla^2 I], \quad (7)$$

where $g(x) = \frac{1}{[1+(s/k)^2]}$, k is a constant. ∇ and Δ are gradient and Laplacian operators, respectively. The advantage of using fourth-order PDE in image denoising is, it removes the blocky effects that made by second-order nonlinearity diffusion equation. However, it requires more number of iterations to converge. Thus, we necessitate a PDE that combines the advantages of second-order and fourth-order partial differential equations.

Pyramid Transform

The image pyramid offers a flexible and convenient multi-resolution format that mirrors the multiple scales of processing in the human visual system. The image pyramid is a data structure designed to support efficient scaled convolution through reduced image representation. It consists of a sequence of copies of an original image in which both sample density and resolution are decreased in regular steps. Pyramid construction is equivalent to convolving the original image with a set of Gaussian-like weighting functions.

A general structure of pyramid transforms consists of decomposition and reconstruction stages and can be described by approximation and interpolation filtering. In the decomposition stage, a signal is successively decomposed into a decimated approximation signal and a signal containing residual information. This residual signal is computed as the difference between the signals on a finer scale and the interpolated signal from a coarser scale. A finer scale corresponds to a lower pyramid layer. The lowest pyramid layer has the same size as the original image. The basic classifications of pyramids are: Gaussian pyramid and Laplacian pyramid. In Gaussian pyramid, the original image G_0 is repeatedly filtered and subsampled to generate the sequence of reduced resolution image G_1, G_2 , etc. These comprise a set of low pass filtered copies of the original image in which the bandwidth decreases in one octave steps. A specific pyramid is determined by its particular decimation factor and approximation and interpolation filters.

In the Laplacian pyramid, two operators REDUCE and EXPAND are commonly used. The REDUCE operator performs a two-dimensional (2D) low pass filtering followed by a subsampling by a factor of two in both directions. The EXPAND operator enlarges an image to twice the size in both directions by up-sampling (i.e., insertion of zeros) and a low pass filtering. The filtering is followed by a multiplication by a factor of 4, which is necessary to maintain

the average intensity being reduced by the insertion of zeros. For an input image I , let its Gaussian pyramid at layer l be G_l , and its Laplacian pyramid at layer 1 be L_l , where $l = 0, 1, 2, \dots, d-1$ and d is the total decomposition layer. The Laplacian pyramid is introduced by Burt and Adelson.³⁹ An important property of the Laplacian pyramid is that it is a complete image representation. The Gaussian and Laplacian pyramids can be defined as

$$\begin{aligned} G_0 &= I, \\ G_l &= \text{REDUCE} [G_{l-1}], \\ L_l &= G_l - \text{EXPAND} [G_{l+1}]. \end{aligned} \quad (8)$$

The Gaussian pyramid consists of a set of low pass filtered copies of the original image at different sizes, whereas the Laplacian pyramid decomposes the original image into a set of band pass images and a final low pass image. Reconstruction of an image from its Laplacian pyramid can be achieved by simply reversing the decomposition steps. The top pyramid level, L_N , is first expanded and added to L_{N-1} to form G_{N-1} then this array is expanded and added to L_{N-2} to recover G_{N-2} , and so on.

MULTISCALE APPROACH

Permutated Diffusion in Laplacian Pyramid Domain

The diffusion coefficients proposed by Zhang,³⁸ Perona and Malik,²¹ Yu and Action²⁴ are ill disposed in the sense that image close to each other are likely to diverge during the diffusion process. Since anisotropic diffusion is designed such that the smooth areas are diffused faster than less smooth ones, blocky effects will appear in the early stage of diffusion, even though all the blocks will finally merge to form a smoother image.

The fourth-order PDE^{40–42} is considered for image denoising for the following reasons, First, Fourth-order linear diffusion dampens oscillations at high frequencies much faster than second-order diffusion. Second, there is the possibility of having schemes that include the effects of curvature in the dynamics, thus creating a richer set of functional behaviors. We have studied a combination of second-order and fourth-order PDE called permutated diffusion that unites the advantages of the second-order and fourth-order PDE. The proposed permutated diffusion avoids the blocky effects caused by second-order PDE, and it requires only minimum number of iterations compared to fourth order; thus, it removes the noise and preserves the edges.

The proposed method consists of three stages as shown in Figure 2. The sequences of operation are: (1) Transformation of an image into its Laplacian pyramid domain, (2) manipulation of pyramid coefficients by regularized permutated diffusion, and (3) reconstruction of the diffused Laplacian pyramid. In the first step, an image is decomposed into its pyramid structure of decreasing frequencies. Pyramid transforms separate information into frequency bands.

Since speckle noise has high frequency, it resides in fine scale corresponds to low pyramid layer. On the other

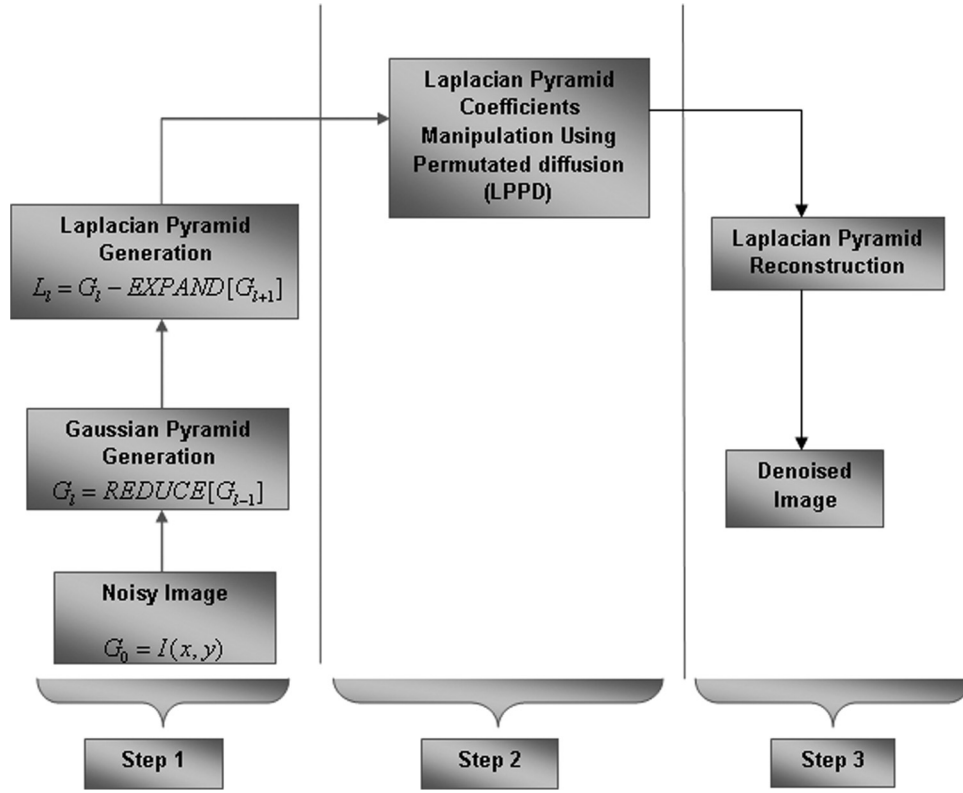


Figure 2. Block diagram of proposed LPPD method.

hand, the speckle noise is negligible in the coarser scale corresponds to the higher pyramid layer. In the second step, each band pass layer of Laplacian pyramid is filtered using regularized permutated diffusion to suppress speckle and to preserve edges. The proposed Laplacian pyramid based permutated diffusion (LPPD) equation is derived as follows:

The heat equation from Fourier’s law of heat flux²² is

$$j(x, t) = -D\nabla I(x, t), \tag{9}$$

where D is a constant. Equation (9) is approximated to a quasihomogeneous system that is near equilibrium and can be approximated as a super flux,

$$j(x, t) = -\sum_q D_q \nabla \nabla^{2q} I(x, t). \tag{10}$$

The energy conservation leads to

$$\frac{\partial I(x, t)}{\partial t} = -\nabla \cdot j(x, t) = \sum_q \nabla \cdot [D_q \nabla \nabla^{2q} I(x, t)]. \tag{11}$$

For an image system it can be expressed as

$$\frac{\partial I(x, y, t)}{\partial t} = -\nabla \cdot [D_1 \nabla I(x, y, t) + D_2 \nabla I(x, y, t) \nabla^2 I(x, y, t)]$$

if $D_1 = D_2 = c(|\nabla I|)$ – Diffusion coefficient,

$$c(|\nabla I|) = \exp\left(-\left[\frac{|\nabla I|}{k}\right]^2\right). \tag{12}$$

And we refer the following equation as permutated diffusion, and it carries both the second and fourth-order terms.

$$\frac{\partial I(x, y, t)}{\partial t} = -\nabla \cdot [c(|\nabla I|) \nabla I(x, y, t) + c(|\nabla I|) \nabla \nabla^2 I(x, y, t)], \tag{13}$$

where ∇ and Δ are gradient and Laplacian operators, respectively. The gradient threshold “ k ” plays an important role in determining the parts of an image that has to be blurred or enhanced in the diffusion process. The diffusion acts as a smoothing filter for large value of k and if k is too low, big noise will be preserved or even amplified instead of being reduced. Thus, the gradient threshold k is estimated using the robust median absolute deviation estimator³⁸

$$k = \frac{c \text{ median } (|\nabla I|)}{0.6745}. \tag{14}$$

The c value is chosen as 1.5 optimally and the mean absolute derivative of zero mean normal distribution with unit variance is 0.6745. The gradient threshold can be represented by

$$k(l) = \frac{1}{0.6745} \text{ median} \left(\frac{|\nabla I(l)|}{\sqrt{2 \log((l+1)/l)}} \right), \tag{15}$$

where l represents the pyramid layer. The image gradient is computed using the pyramid coefficients in the

corresponding pyramid layer. In this method, a relatively large value is used in the lowest pyramid layer where speckle is dominant and in order to remove it more thoroughly. On the other hand, to preserve structure boundaries a small gradient threshold is applied in higher layers. In the third step, the image is reconstructed from its Laplacian pyramid by simply reversing the decomposition steps.

Numerical Implementation of Permutated Diffusion in Pyramid Domain

A finite difference scheme is chosen to solve the diffusion equation because of its easy implementation. Let the time step be Δt and the spatial step be h in x and y directions. Then, the time and space coordinates can be discretized as

$$\begin{aligned} t &= n\Delta t, n = 0, 1, 2, \dots, \\ x &= ih, y = jh, \\ i &= 0, 1, 2, 3, \dots, M-1, \\ j &= 0, 1, 2, 3, \dots, N-1 \text{ and } h = 1, \end{aligned}$$

where $Mh \times Nh$ is the size of the image support and let $I_{i,j}^n = I(ih, jh, n\Delta t)$. The image gradients are obtained from directional differences

$$\begin{aligned} \nabla I_N^n(i, j) &= I_{i-1,j}^n - I_{i,j}^n, \\ \nabla I_S^n(i, j) &= I_{i+1,j}^n - I_{i,j}^n, \\ \nabla I_W^n(i, j) &= I_{i,j-1}^n - I_{i,j}^n, \\ \nabla I_E^n(i, j) &= I_{i,j+1}^n - I_{i,j}^n, \end{aligned} \quad (16)$$

with symmetric boundary condition,

$$\begin{aligned} I_{-1,j}^n &= I_{0,j}^n, \quad I_{I+1,j}^n = I_{I,j}^n, \quad j = 0, 1, 2, 3, \dots, J, \\ I_{i,-1}^n &= I_{i,0}^n, \quad I_{i,I+1}^n = I_{i,0}^n, \quad i = 0, 1, 2, 3, \dots, I, \end{aligned}$$

$|\nabla I|$ is discretized as the average of the four squared directional differences and the gradient magnitude is given by

$$|\nabla I| = 0.5 \times \sqrt{|\nabla I_N|^2 + |\nabla I_S|^2 + |\nabla I_W|^2 + |\nabla I_E|^2}. \quad (17)$$

The diffusion coefficient in Eq. (12) can be calculated from

$$\begin{aligned} C_N^n(i, j) &= c(|\nabla I_N^n(i, j)|), \\ C_S^n(i, j) &= c(|\nabla I_S^n(i, j)|), \\ C_W^n(i, j) &= c(|\nabla I_W^n(i, j)|), \\ C_E^n(i, j) &= c(|\nabla I_E^n(i, j)|), \end{aligned} \quad (18)$$

with symmetric boundary condition

$$\begin{aligned} c_{-1,j}^n &= c_{0,j}^n, \quad c_{I+1,j}^n = c_{I,j}^n, \quad j = 0, 1, 2, 3, \dots, J, \\ c_{i,-1}^n &= c_{i,0}^n, \quad c_{i,I+1}^n = c_{i,0}^n, \quad i = 0, 1, 2, 3, \dots, I. \end{aligned}$$

The Laplacian can be discretized as

$$\nabla^2 I_{i,j}^n = I_{i+1,j}^n + I_{i-1,j}^n + I_{i,j+1}^n + I_{i,j-1}^n - 4I_{i,j}^n. \quad (19)$$

If we define $g_{i,j}^n = c(|\nabla I_{i,j}^n|) \nabla I_{i,j}^n$, then,

$$\begin{aligned} g_{i,j} &= c_N^n(i, j) \nabla I_N^n(i, j) + c_S^n(i, j) \nabla I_S^n(i, j) \\ &+ c_W^n(i, j) \nabla I_W^n(i, j) + c_E^n(i, j) \nabla I_E^n(i, j). \end{aligned} \quad (20)$$

The permutated diffusion can be expressed as

$$I_{i,j}^{n+1} = I_{i,j}^n + \lambda [g_{i,j}^n + g_{i,j}^n \nabla^2 I_{i,j}^n], \quad (21)$$

where λ is the time step and controls the speed of diffusion. To solve the permutated diffusion, the Neumann boundary condition is imposed in which it is assumed that the values beyond an image border are equivalent to values on the border. Multiscale processing performs local operation to produce global effects, and it requires much smaller number of iterations as compared to single scale processing method. Thus, the time step is chosen as $\lambda \leq 0.25$.

Stopping Criteria

As the diffusion process is iterative, one challenging task is deciding when the diffusion process is to be stopped. It can be stopped manually by setting a fixed number of iterations. However, in real applications, different images may need different numbers of diffusion iterations. Thus, a mechanism to stop the diffusion automatically is preferred. The mean absolute error (MAE) between two adjacent diffusion steps can be used to stop the iteration.

$$\text{MAE}(I(t)) = \frac{1}{M \times N} \sum_{(i,j)=1}^{M,N} \sqrt{(I(i, j, t) - I(i, j, t-1))^2}, \quad (22)$$

where $I(i, j, t)$ and $I(i, j, t-1)$ are the filtered values of the pixel (i, j) at time t and $t-1$, respectively, and M, N are the numbers of columns and rows in the processed image, respectively.

The convergence of nonlinear diffusion process depends on the numerical scheme, image size and diffusivity functions.⁴³ In our method, we have incorporated explicit discretization scheme. The stability requirement for this scheme is the time step λ should be $\leq 1/2D$, where D is number of dimensions along which the gradient value is measured and is equal to 2 for image, i.e., $\lambda \leq 0.25$. Multiscale processing performs local operation to produce global effects.⁴⁴ In our study, we have determined MAE values for FIELD II software simulated test phantom by applying permutated diffusion to three band pass layers and MAE value decrease exponentially with the number of iterations as shown in Figure 3. By setting a threshold value for MAE, iterations can be stopped and according to the purpose of speckle reduction, the threshold value can be adjusted by the clinicians.

EXPERIMENT RESULTS AND DISCUSSION

The performance of the proposed method is evaluated using simulated phantom and real ultrasound images. In each study, the performance of proposed LPPD is compared with Laplacian pyramid based nonlinear diffusion (LPND),

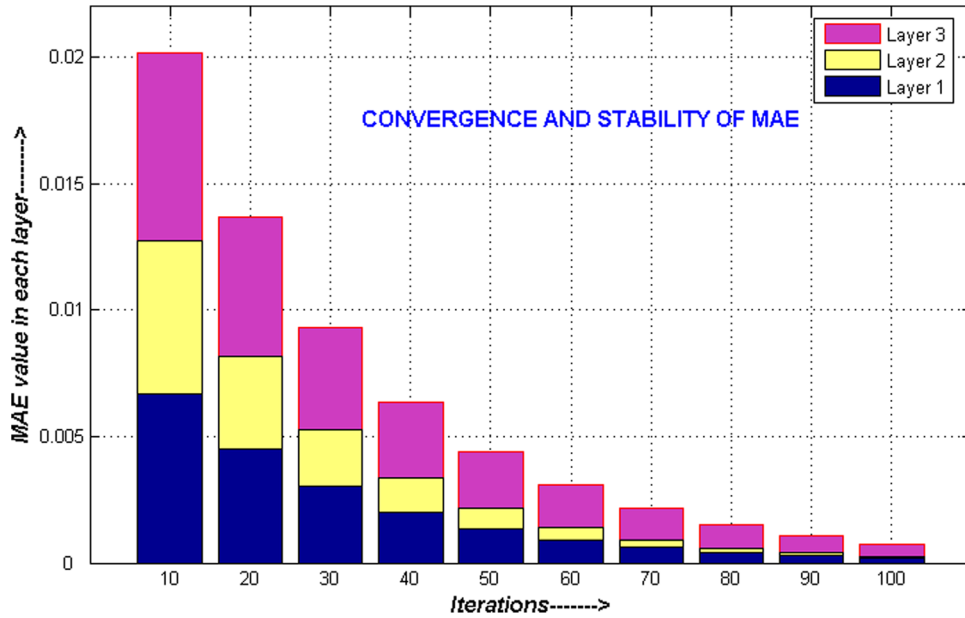


Figure 3. Stability and convergence of MAE.

Laplacian pyramid based Wiener filter (LPWF), nonlinear coherent diffusion (NCD), SRAD, and Gaussian regularized nonlinear diffusion (GRND). To quantify the performance, three metrics are computed, first, the figure of merit (FOM) is used as edge-preserving measure that is defined as³⁸

$$FOM = \frac{1}{\max\{\hat{N}, N_{ideal}\}} \sum_{i=1}^N \frac{1}{1 + d_i^2 \lambda} \quad (23)$$

In this equation, N and N_{ideal} are the numbers of detected and original edge pixels, respectively; d_i is the Euclidean distance between the i th detected edge pixel and the nearest original edge pixel; λ is a constant typically set to 1/9. The dynamic range of FOM is between the processed image and

the ideal image. We have used the Canny edge detector²⁴ to find the edge in all processed results. Second, the structural similarity index (SSIM) models any distortion as a combination of three different factors:⁴⁵ loss of correlation, luminance distortion, and contrast distortion.

$$SSIM = Q = Q_1 Q_2 Q_3 = \frac{\sigma_{xy}}{\sigma_x \sigma_y} \times \frac{2\bar{X}\bar{Y}}{(\bar{X})^2 + (\bar{Y})^2} \times \frac{2\sigma_x \sigma_y}{\sigma_x^2 + \sigma_y^2} \quad (24)$$

The first component is the correlation coefficient between x and y , which measures the degree of linear correlation between x and y , and its dynamic range is $[-1,1]$. The best value 1 is obtained when $y_i = ax_i + b$ for all $i = 1, 2, \dots, N$,

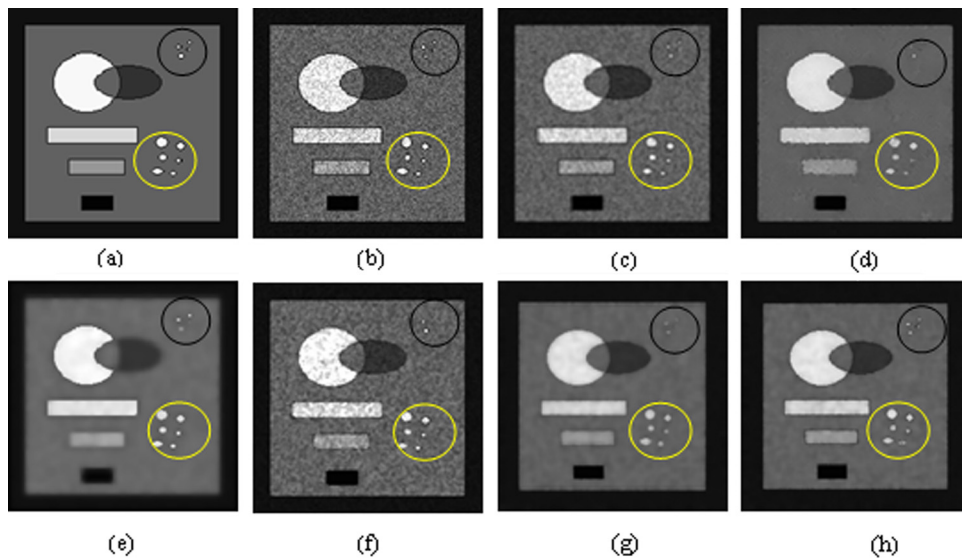


Figure 4. Simulated B mode image and its filtered results (a) echogenicity map (b) speckled image with variance 0.05 (c)-(h) image filtered by NCD, SRAD, GRND, LPWF, LPND, and LPPD.

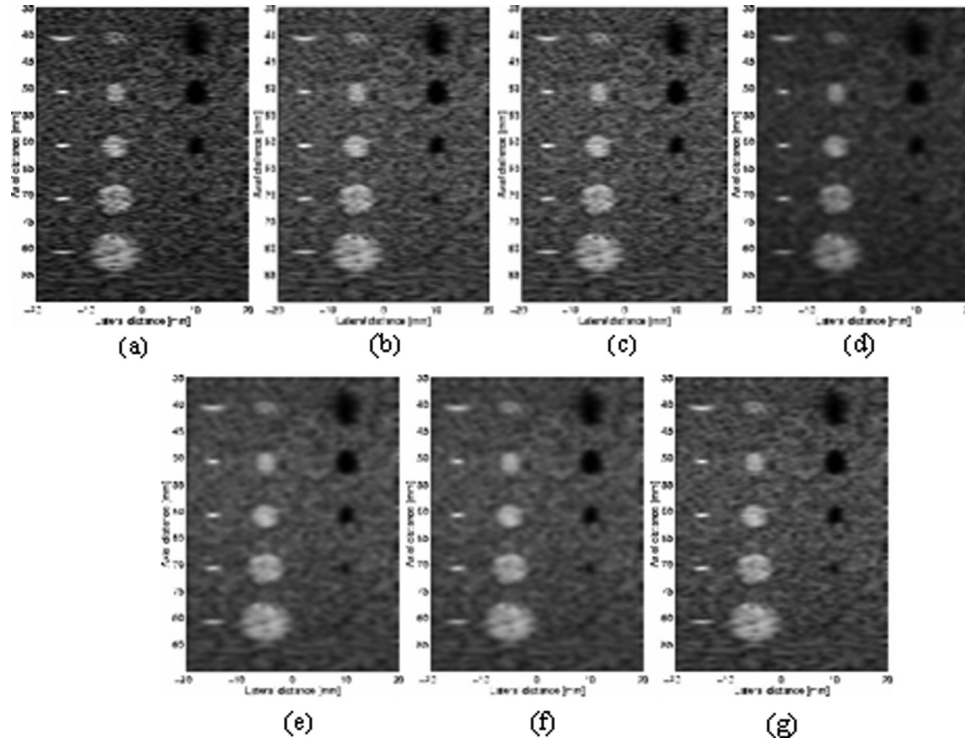


Figure 5. FIELD II simulated B mode image: (a) cyst image (b)–(g) images filtered by NCD, SRAD, GRND, LPVWF, LPND, and LPPD.

where a and b are constants and $a > 0$. Even if x and y are linearly related, there still might be relative distortions between them, which are evaluated in the second and third components. The second component, with a value range of $[0, 1]$, measures how much the x and y are close in luminance. It equals 1 if and only if $X = Y$. σ_x and σ_y can be viewed as an estimate of the contrast of x and y , so the third component measures the similarities between the contrasts

of the images. Its range of values is also $[0, 1]$, where the best value 1 is achieved if and only if $\sigma_x = \sigma_y$.

Third the edge preservation index (EPI)⁴⁶ is used as measure of edge preservation.

$$EPI = \frac{\sum (\Delta s - \Delta \bar{s})(\Delta \hat{s} - \Delta \bar{\hat{s}})}{\sqrt{\sum (\Delta s - \Delta \bar{s})^2 \sum (\Delta \hat{s} - \Delta \bar{\hat{s}})^2}}, \quad (25)$$

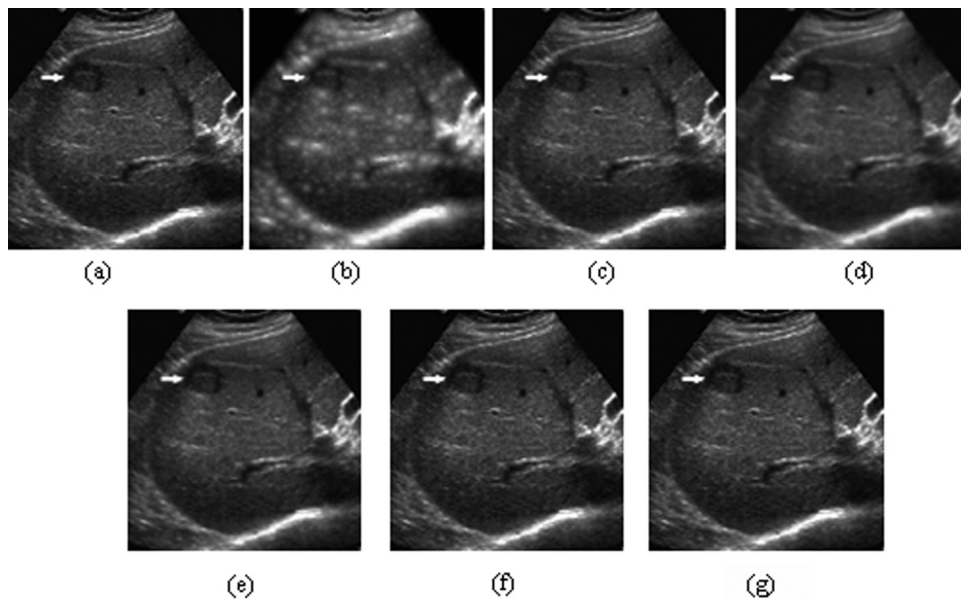


Figure 6. Real ultrasound image and its filtered results: (a) ultrasound image (b)–(g) images filtered by NCD, SRAD, GRND, LPVWF, LPND, and LPPD.

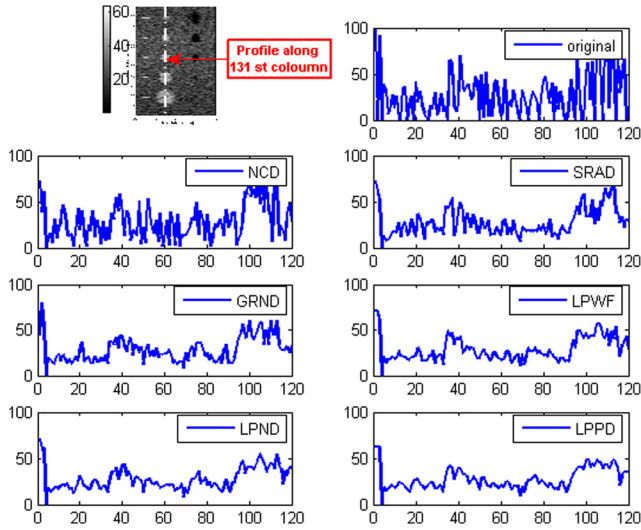


Figure 7. Image profile along 131st column of simulated phantom.

where s and \hat{s} are the original and denoised images respectively, \bar{s} shows mean of s , and Δs is the high pass filtered s using the discrete Laplacian operator. The results of various methods on simulated B mode image for the speckle noise of variance 0.05 are shown in Figures 4(a)–4(h). In this study, for SRAD implementation, the time step $\Delta t = 0.05$ is chosen, and 300 iterations are used. For LPND, four pyramid layers, 7×7 binomial filter for REDUCE and EXPAND operator, the Gaussian filter of $\sigma = 0.1$, $\Delta t = 0.2$, and MAE = 0.1 is set.

For NCD $\Delta t = 3$, $\alpha = 1$, $s = 70$, and $\beta = 0.05$ are selected. For GRND and LPWF, the filter mask of 5×5 , median filter with $\sigma = 2$ and $\Delta t = 0.2$ are utilized. In LPPD, the point features linear features enclosed by blue, red circles are enhanced, and the noise is suppressed to the maximum level and gives visually improved results.

The performance of proposed method and other approaches on FIELD II software generated cyst which is shown in Figure 5. FIELD II version 3.16 is used to simulate

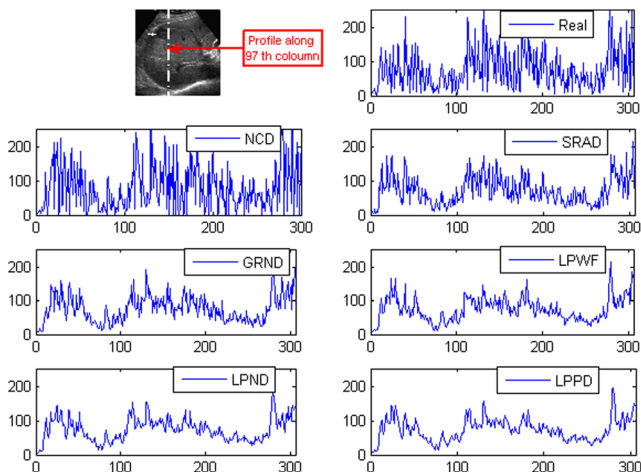


Figure 8. Image profile along 97th column of real ultrasound image.

Table I. FOM, SSIM, and EPI values for simulated phantom using various methods.

	For simulated image		
	FOM	SSIM	EPI
Noisy/Real	0.083	0.3543 ± 0.0042	0.613
NCD	0.108	0.7368 ± 0.0043	0.673
SRAD	0.198	0.7546 ± 0.0045	0.734
GRND	0.116	0.7481 ± 0.0039	0.823
LPWF	0.683	0.7763 ± 0.0042	0.856
LPND	0.728	0.7289 ± 0.0038	0.897
LPPD	0.902	0.8237 ± 0.0041	0.944

B-mode ultrasound image^{47,48} of cyst. The cyst consists of a background class in gray with pixel value 1, five bright and dark objects in white, black are aligned vertically with pixel value 5 and 0, respectively. The parameters used for the simulation of cyst are: transducer center frequency-3.5 MHz, sampling frequency-100 MHz, and speed of sound-1540 m/s, wavelength-0.44 mm, element width-0.44 mm, element height-5 mm, focal point-70 mm, number of physical elements-192, and number of active elements-64.

The cyst phantom is an 8 bit image of size 390×500 pixels composed of five dark and bright objects of various sizes. Our proposed method LPPD gives a good visual enhancement and preserves small structures. Figure 6 gives the performance of proposed method and other approaches on real ultrasound data set.

Figure 7 gives performance of various methods in terms of image profile along 131st column in the cyst phantom. The performance analysis in terms of image profile on real ultrasound data along the 97th column is given in Figure 8. FOM, EPI, and SSIM are calculated for each filtered image. The metric values for simulated phantom and real ultrasound data set are listed in Tables I and II. The graphical comparison is shown in Figure 9.

Compared to other approaches LPPD shows the most noise reduction while preserving small structures, the six small cysts and four point targets. LPND shows sharper but

Table II. FOM, SSIM, and EPI values for real ultrasound image using various methods.

	For real ultrasound data		
	FOM	SSIM	EPI
Noisy/Real	0.089	0.3743 ± 0.0042	0.658
NCD	0.118	0.7309 ± 0.0043	0.709
SRAD	0.188	0.7586 ± 0.0036	0.764
GRND	0.124	0.7581 ± 0.0039	0.887
LPWF	0.692	0.7793 ± 0.0048	0.890
LPND	0.808	0.7989 ± 0.0038	0.897
LPPD	0.913	0.8437 ± 0.0041	0.964

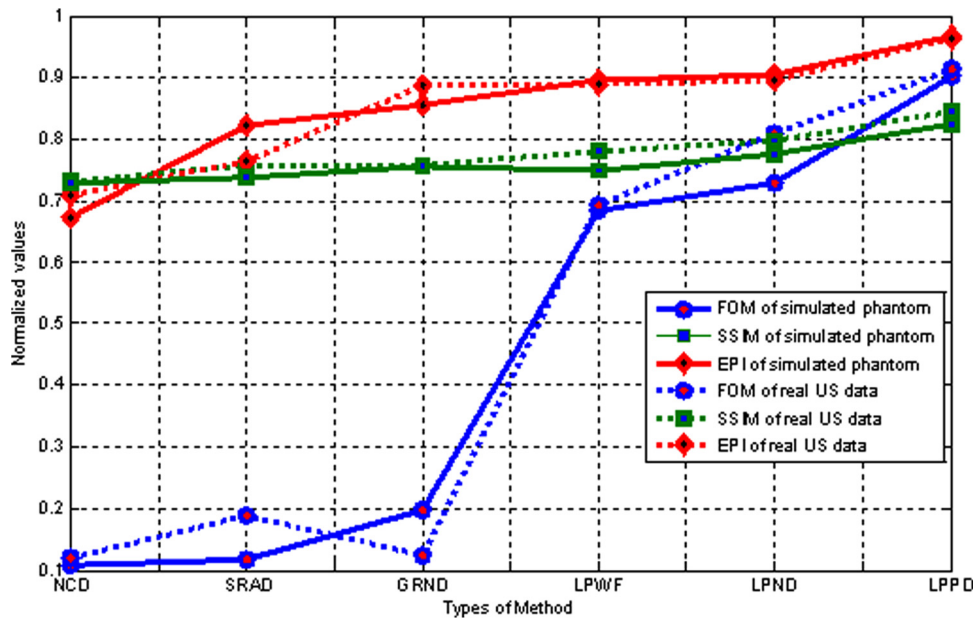


Figure 9. Comparison performance on simulated and real ultrasound data set using various methods.

jagged edges and gives a relatively low contrast. LPWF does not give satisfactory speckle suppression. NCD enhances edges but it does not keep correct edge locations with the SRAD, the boundaries of bright regions are broadened and those of dark regions are shrunk. GRND enhances the edge coherence but cannot suppress enough noise.

CONCLUSION

The proposed method is mainly focused on producing simplified ultrasound images for subsequent computer-assisted image analysis such as automatic or semiautomatic segmentation and registration, although it can also provide a visual diagnostic aid for clinicians to interpret ultrasound images. In this multiresolution approach, the permuted diffusion of second-order and fourth-order PDE is regularized by a median regulator to guide energy source and to boost the features in the image. In each pyramid layer, a gradient threshold is estimated automatically using robust median estimator. The MAE between two adjacent diffusion steps is used as stopping criterion. It removes noise and keeps the edge by little iteration. Experiment results indicate this method has better satisfactory performance in terms of speckle reduction, detail preservation and improved visual enhancement than other methods. Furthermore, it can be easily implemented and robust.

REFERENCES

- Achim, A. Bezerianos, and T. Tsakalides, "Novel Bayesian multiscale method for speckle removal in medical ultrasound images," *IEEE Trans. Med. Imaging* **20**, 772–783 (2001).
- C. B. Burckhardt, "Speckle in ultrasound B-mode scans," *IEEE Trans. Sonics Ultrason.* **25**, 1–6 (1987).
- J. W. Godman, "Some fundamental properties of speckle," *J. Opt. Soc. Am.* **66**, 1145–1150 (1976).
- R. F. Wagner, S. W. Smith, and J. M. Sandrik, "Statistics of speckle in ultrasound B-scans," *IEEE Trans. Sonics Ultrason.* **30**, 156–163 (1983).
- Karmeshu and R. Agrawal, "Study of ultrasonic echo envelope based on Nakagami-inverse Gaussian distribution," *Ultrasound Med. Biol.* **32**, 371–376 (2003).
- P. M. Shankar, "Ultrasonic tissue characterization using a generalized Nakagami model," *IEEE Trans. Ultrason. Ferroelectr. Freq. Control* **48**, 1716–1720 (2001).
- T. Eltoft, "Modeling the amplitude statistics of ultrasonic images," *IEEE Trans. Med. Imaging* **25**, 229–240 (2006).
- M. O. Donnel and S. D. Silverstein, "Optimum displacement for compound image generation in medical Ultrasound," *IEEE Trans. Ultrason. Ferroelectr. Freq. Control* **35**, 470–476 (1988).
- G. E. Trahey, J. W. Allison, S. W. Smith, and O. T. Von Ramm, "A quantitative approach to speckle reduction via frequency compounding," *Ultrasound. Imaging* **8**, 151–164 (1986).
- P. C. Lie and M. J. Chen, "Strain compounding: A new approach for speckle reduction," *IEEE Trans. Ultrason. Ferroelectr. Freq. Control* **49**, 39–46 (2002).
- J. C. Bamber and C. Daft, "Adaptive filtering for reduction of speckle in ultrasound pulse echo images," *Ultrasonics* **24**, 41–44 (1986).
- V. Dutt and J. F. Greenleaf, "Adaptive speckle reduction filter for log compressed B-scan images," *IEEE Trans. Med. Imaging* **15**, 802–813 (1996).
- J. I. Koo and S. B. Park, "Speckle reduction with edge preservation in medical ultrasonic images using a homogeneous region growing mean filter (HRGMF)," *Ultrason. Imaging* **13**, 211–237 (1991).
- M. Karaman, M. A. Kutay, and G. Bozdagi, "An adaptive speckle suppression filter for medical ultrasonic imaging," *IEEE Trans. Med. Imaging* **14**, 283–292 (1995).
- H. C. Haung, J. Y. Chen, S. D. Wang, and C. M. Chen, "Adaptive ultrasonic speckle reduction based on the slope facet model," *Ultrasound Med. Biol.* **29**, 1161–1175 (2003).
- R. Touzi, "A review of speckle filtering in the context of estimation theory," *IEEE Trans. Geosci. Remote Sens.* **40**, 2392–2404 (2002).
- J. Lee, "Digital image enhancement and noise filtering using local statistics," *IEEE Trans. Pattern Anal. Mach. Intell.* **2**, 165–168 (1980).
- V. Frost, J. Stiles, K. Shanmugan, and J. Holtzman, "A model for radar images and its application to adaptive digital filtering of multiplicative noise," *IEEE Trans. Pattern Anal. Mach. Intell.* **4**, 157–166 (1982).
- D. T. Kuan, A. A. Sawchuk, T. Strand, and P. Chavel, "Adaptive restoration of images with speckle," *IEEE Trans. Acoust., Speech, Signal Process.* **35**, 373–383 (1987).
- D. T. Kuan, A. A. Sawchuk, T. C. Strand, and P. Chavel, "Adaptive noise smoothing filter for images with signal-dependent noise," *IEEE Trans. Pattern Anal. Mach. Intell.* **7**, 165–177 (1985).
- P. Perona and M. Malik, "Scale-space and edge detection using anisotropic diffusion," *IEEE Trans. Pattern Anal. Mach. Intell.* **12**, 629–639 (1990).

- ²²G. W. Wei, "Generalized Perona–Malik equation for image restoration," *IEEE Signal Process. Lett.* **6**, 165–167 (1999).
- ²³T. Chan, A. Marquina, and P. Mulet, "Higher order total variation based image restoration," *SIAM J. Sci. Comput. (USA)* **22**, 503–516 (2000).
- ²⁴Y. Yu and S. Acton, "Speckle reducing anisotropic diffusion," *IEEE Trans. Image Process.* **11**, 1260–1270, (2002).
- ²⁵M. R. Banham and A. G. Katsaggelos, "Digital image restoration," *IEEE Signal Process. Mag.* **14**, 24–41 (1997).
- ²⁶C. R. Vogel and M. E. Oman, "Fast, robust total variation-based reconstruction of noisy, blurred images," *IEEE Trans. Image Process.* **7**, 813–824 (1998).
- ²⁷P. Charbonnier, L. Blanc-Féraud, G. Aubert, and M. Barlaud, "Edge-preserving regularization in computed imaging," *IEEE Trans. Image Process.* **6**, 298–310 (1997).
- ²⁸M. I. H. Bhuiyan, M. O. Ahmad, and M. N. S. Swamy, "Spatially adaptive thresholding in wavelet domain for despeckling of ultrasound images," *IET Image Process.* **3**, 147–162 (2009).
- ²⁹A. H. Delaney and Y. Bresler, "Globally convergent edge-preserving regularized reconstruction: An application to limited-angle tomography," *IEEE Trans. Image Process.* **7**, 204–221 (1998).
- ³⁰L. Lin, Y. Wang, and H. Zhou, "Iterative filtering as an alternative algorithm for empirical mode decomposition," *Adv. Adaptive Data Anal.* **1**, 543–560 (2009).
- ³¹P. Coupe, P. Hellier, C. Kervrann, C. Barillot, "Nonlocal means-based speckle filtering for ultrasound images," *IEEE Trans. Image Process.* **18**, 2221–2229 (2009).
- ³²X. Zong, A. F. Laine, and E. A. Geiser, "Speckle reduction and contrast enhancement of echocardiograms via multiscale nonlinear processing," *IEEE Trans. Med. Imaging* **17** 532–540 (1998).
- ³³X. Hao, S. Gao, and X. Gao, "A novel multiscale nonlinear thresholding method for ultrasonic speckle suppressing," *IEEE Trans. Med. Imaging* **18**, 787–794 (1999).
- ³⁴H. Xie, V. Pierce, and F. T. Ulaby, "SAR speckle reduction using wavelet denoising and Markov random field modeling," *IEEE Trans. Geosci. Remote Sen.* **40**, 2196–2212 (2002).
- ³⁵N. Gupta, M. N. S. Swamy, and E. Plotkin, "Despeckling of medical ultrasound images using data and rate adaptive lossy compression," *IEEE Trans. Med. Imaging* **24**, 743–754 (2005).
- ³⁶A. Pizurica, W. Philips, I. Lemahieu, and M. Achero, "A versatile wavelet domain noise filtration technique for medical imaging," *IEEE Trans. Med. Imaging* **22**, 323–331 (2003).
- ³⁷B. Aiazzi, L. Alparone, S. Baronti, and F. Lotti, "Multiresolution local statistics speckle filtering based on a ratio Laplacian pyramid," *IEEE Trans. Geosci. Remote Sen.* **36**, 1466–1476 (1998).
- ³⁸F. Zhang, L. M. Koh, Y. M. Yoo, and Y. Kim, "Nonlinear diffusion in Laplacian pyramid domain for ultrasonic speckle reduction," *IEEE Trans. Med. Imaging* **26**, 200–211 (2007).
- ³⁹P. J. Burt and E. A. Adelson, "The Laplacian pyramid as a compact image code," *IEEE Trans. Commun.* **31**, 532–540 (1983).
- ⁴⁰Y. L. You and M. Kaveh, "Fourth-order partial differential equations for noise removal," *IEEE Trans. Image Process.* **9**, 1723–1730 (2000).
- ⁴¹M. Lysaker, A. Lundervold, and X. C. Tai, "Noise removal using fourth-order partial differential equation with application to medical magnetic resonance images in space and time," *IEEE Trans. Image Process.* **12**, 1579–1590 (2003).
- ⁴²G. W. Wei and Y. Q. Jia, "Synchronization based image edge detection," *Europhys. Lett.* **59**, 814 (2002).
- ⁴³S. T. Acton, "Multigrid anisotropic diffusion," *IEEE Trans. Image Process.* **7**, 280–291 (1998).
- ⁴⁴P. Mrázek, J. Weickert, G. Steidl, and M. Welk, "On iterations and scales of nonlinear filters," in *Proc. Computer Vision Winter Workshop*, edited by O. Drbohlav (Valtice, Czech Republic, 2003), pp. 61–66.
- ⁴⁵W. K. Pratt, *Digital Image Processing* (Wiley, New York, NY, 1978).
- ⁴⁶Z. Wang, A. C. Bovik, H. R. Sheikh, and E. P. Simoncelli, "Image quality assessment: From error visibility to structural similarity," *IEEE Trans. Image Process.* **13**, 600–612 (2004).
- ⁴⁷J. A. Jensen and N. B. Svendsen, "Calculation of pressure fields from arbitrarily shaped apodized and excited ultrasound transducers," *IEEE Trans. Ultrason. Ferroelectr. Freq. Control* **39**, 262–267 (1992).
- ⁴⁸J. A. Jensen, "Field: A program for simulating ultrasound systems," *Med. Biol. Eng. Comput.* **34**, 351–353 (1996).